Proton-exchange membrane fuel cell design for in-situ depth-sensitive X-ray absorption spectroscopy

Michal Ronovský, Mila Myllymäki, Yves Watier, Pieter Glatzel, Peter Strasser, Alex Martinez Bonastre, Jakub Drnec

Proton-exchange membrane fuel cell design for in-situ depth-sensitive X-ray absorption spectroscopy

Michal Ronovsky[1, 3], Mila Myllymaki[2], Yves Watier[1], Pieter Glatzel[1], Peter Strasser[3], Alex Martinez Bonastre[4], Jakub Drnec[1]*

[1] *ESRF—The European Synchrotron, ID31 Beamline, Grenoble, France*

[2] *University of Helsinki, Helsinki, Finland*

[3] *Technical University Berlin, Berlin, Germany*

[4] *Johnson Matthey Technology Centre, Blount's Court, Sonning Common, Reading RG4 9NH, U.K.*

** corresponding author: Jakub Drnec, drnec@esrf.fr*

Abstract

We have built a proton exchange membrane hydrogen fuel cell optimized for angle-resolved X-ray absorption spectroscopy. This cell allows in-situ fluorescence measurements during electrochemical operation with minimal trade-offs in cell performance while reaching automotive current densities. The fluorescence signal can be collected from wide angles to extract depth information from the probed atomic species such as Pt, Co, and Ni, crucial to highly efficient FC. This cell is designed to assess the connection between the ionic drag/diffusion and the performance loss by following the real-time movement of the species through the membrane electrode assembly.

Keywords

XAS, PEMFC, cation poisoning, cell design, depth-profiling

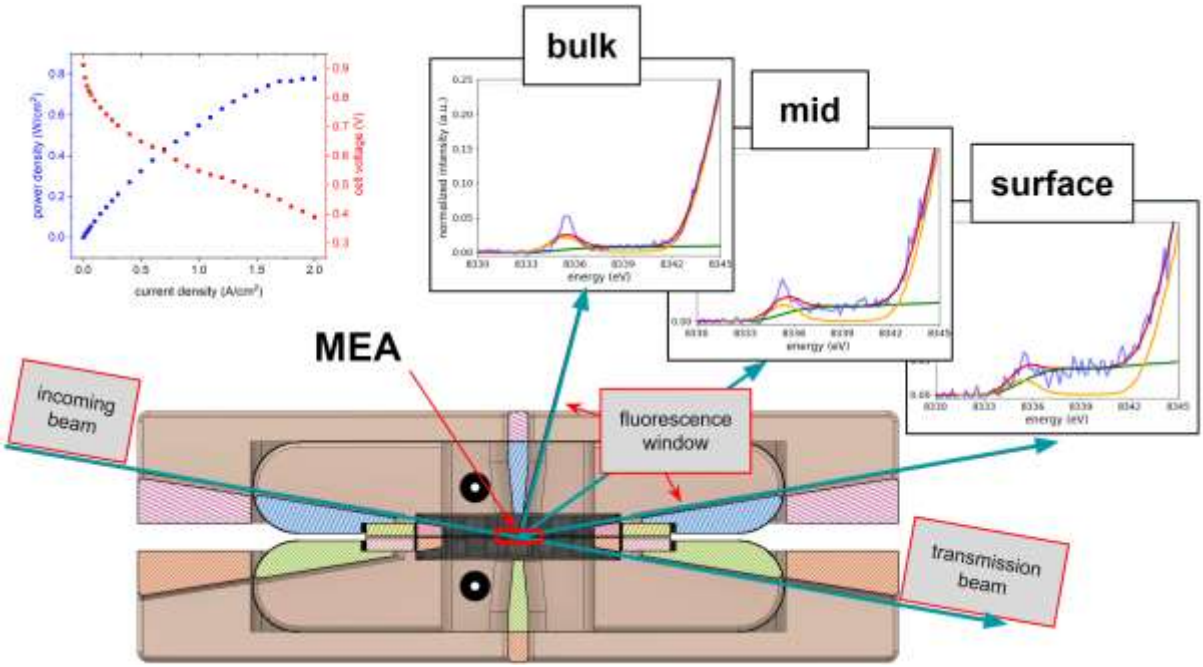

Introduction

The growing demand for clean energy technology drives the development of proton-exchange hydrogen fuel cells (PEMFCs). Due to their higher activity towards oxygen reduction reaction (ORR), platinum alloys with transition metals such as Ni or Co have the potential to improve PEMFC performance significantly [1]. However, incorporating these alloys brings additional challenges as they are prone to leaching the secondary metal. Dissolved atoms migrate and diffuse into the ionomer within the catalyst layer and the proton conductive membrane, blocking the proton channels, increasing proton transport resistance, and thus decreasing the performance [2]. To understand the mechanisms and dynamics of ionomer poisoning, an effective operando experimental approach has to be developed.

X-ray absorption spectroscopy (XAS) has proven its use for monitoring catalyst species due to its sensitivity to oxidation states [3]. While a half-cell design from S. Mukerjee's team has pushed the field forward from standard liquid cells [4], only a handful of XAS-optimized hydrogen fuel cell designs were published. The most common approach is to thinner graphite flowfields that the XAS signal can penetrate [5], [6], [7]. The latest cell from Principi et al. [8] uses a flowfield thinned to 250 nm at one place. Where this cell offers a good transmission coefficient of 90% at 10 keV and 50% at 9 keV, the flowfields are too thick for usage at lower photon energies. The attenuation has to be compensated with high loadings, and even one of the latest works with this type of cell uses a cathode catalyst with 4 mg_{Pt}/cm^2 [9]. Ishiguro et al. advanced with a time-resolved XAS measurement on Pt_3Co and Pt_3Ni catalysts with loadings of 0.5 mg_{metal}/cm^2 even though Co and Ni K-edges are at significantly lower energies than Pt L-edge [10]. However, even such loadings are high compared to the current DOE target of 0.125 mg_{Pt}/cm^2 on both electrodes combined [11] and it is therefore becoming clear that this standard approach is not feasible anymore for current state-of-the-art ORR catalysts. An advanced design comprising a PET-film window has succeeded in probing sulfur K-edge as low as 2.4 keV [12].

Getting information about the oxidation state is one thing, but investigating the dynamics of ionomer poisoning requires depth sensitivity. Baker et al. [13] developed an operando confocal microprobe to investigate the spatial distribution of Ce ions in the membrane electrode assembly (MEA). In their system, the MEA is cut and sealed with Kapton at the edge. Despite very challenging data reconstruction, they were able to describe the dynamic behavior of Ce inside the CCM stack when changing from OCP to constant current. Similarly, Matsui et al. [14] have performed impressive 3D computed XAS tomography. However, using imaging techniques requires a large number of data points, and thus, only a few emission energies are recorded to prevent beam damage. Consequently, the signal-to-noise ratio is drastically lowered compared to standard techniques, making reliable deconvolution of various oxidation states difficult (if not impossible).

Another way to get depth information is to use XAS while varying either incidence and/or emission angles [15]. Only a few experiments were reported using such a technique in the fluorescence mode [16], [17]. However, they were conducted in a liquid cell and planar configuration, which is inherently different from a real device. Gunduz et al. tried an analogous experiment with a button cell for ammonia production [18]. Yet, as they also rightly pointed out, the penetration depth of the incoming X-rays depends on the energy of

the incoming beam, with the difference between the attenuation coefficients pre- and post-edge being up to one order of magnitude. This significantly complicates the depth-data interpretation when the experiment is designed to change the incidence angle while probing the absorption edge.

Our approach to both cell design and experiment setup aims to combine the advantages of using a Kapton window with the channel in the flowfield as direct access to the MEA and a high-resolution angle-resolved XAS. With the former, we investigate low-loading (< 0.1 mg_{Pt}/cm^2) catalysts as X-ray absorption occurs only on the thin Kapton foil and the MEA itself. The latter is inherently depth-sensitive and allows for conventional XAS data analysis approaches, e.g., linear combination fitting or principal component analysis. Additionally, we keep the incidence angle constant and acquire high-resolution XAS spectra in the fluorescence mode at different emission angles with a multi-crystal analyzer.

Here, we describe an operando PEMFC optimized for angle-resolved X-ray absorption spectroscopy to study the origin of metallic species with the option of obtaining depth information from each species with a different oxidation state and reaching current densities of more than 1 A/cm^2. We acquire the XAS signal from the Ni K-edge with the Ni loading of just 0.017 mg_{Ni}/cm^2. The main advance in our design is using the channel in a flow field as direct access to the MEA and a unique experimental setup. This way, we probe the MEA in-situ/operando without compromising the electrochemical environment.

Results

PEM fuel cell design

The symmetrical cell, as illustrated in Figure 1a, comprises a two-part copper body with a Kapton window, a graphite flowfield, a rubber gasket, and a resin heat shield. This design allows both absorption and fluorescence X-ray measurements.
Copper Body Parts: The cell incorporates two copper body parts. The outer part features two intrusions for heating cartridges and holes for cell compression using 3 mm screws (Figure 1b). The inner body is wrapped with Kapton tape, which provides electrical insulation, a gas-tight seal, and, most importantly, acts as a window for X-rays, enabling the acquisition of low-energy fluorescence from low-loading electrodes.
Graphite Flowfield and Rubber Gasket: The inner body contains a mortise to accommodate the graphite flowfield and a rubber gasket. The graphite flowfield has a specially designed (1 x 2) mm channel in the middle, as depicted in Figure 1c, through which X-rays reach and leave the membrane electrode assembly. Adjacent to the channel are two lands of the same size, providing a total active area of 6 mm^2 (marked in green). This small sample size is beneficial for laboratory-scale research, limited by the small amount of synthesized catalysts and, thus, the availability of CCMs.
Resin Heat Shield: Once compressed, the cell is inserted into a resin heat shield (Figure 1b). It minimizes heat loss, improves thermal homogeneity within the cell, and prevents the formation of cold spots and vapor condensation that could impact performance.
Groove Design: The outer and inner body parts feature a 2 mm groove in the middle, ranging from 9° to 81° from the cell's center with respect to the sample plane (Figure 1a, d).

This deliberate design enhances the signal-to-noise ratio and allows X-ray fluorescence to be captured at different emission angles, thus capturing depth information. Additionally, the bridge in the middle acts as a structural support once the cell is compressed and facilitates water droplet removal by directing the flow of gasses through the channel.

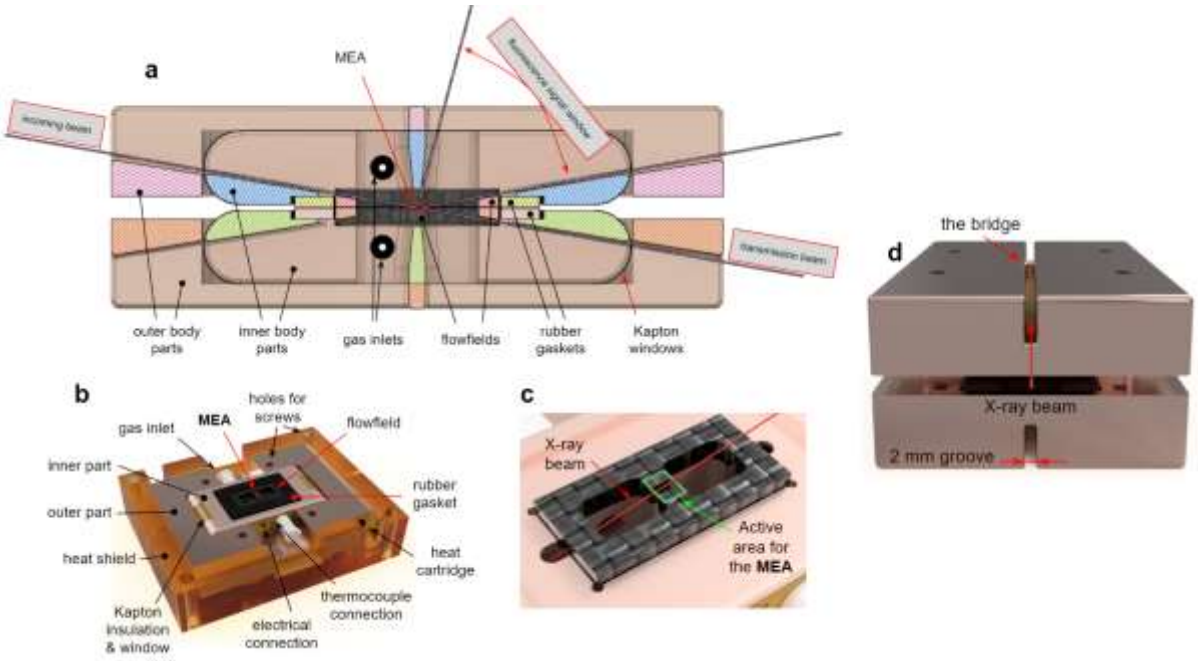

Figure 1: a) a cross-sectional cut through the middle of the cell: hatched areas correspond to a material being cut by the section plane; b) the bottom half of the symmetrical cell with the resin heat shield; c) a detail of the flowfield with active area for the MEA composed of one (1 x 2) mm channel and two adjacent lands marked in green; d) a view along the beam path on the assembled cell (without the heat shield), 2 mm groove in the middle for X-rays emission.

Electrochemical characterization

The performance of the cell was tested with a PtNi-based catalyst. Operating at 80°C, flowing 3/2 sccm of H_2/O_2 on anode/cathode, respectively, with 50% relative humidity and 0.1 bar backpressure. We reach 2 A/cm^2 at 0.39 V (Figure 2a). Under these conditions, the cell runs stably (Figure 2b). PEIS in Figure 2c shows a reasonable ohmic resistance of 1.7 Ohms. Standard cyclic voltammetry (Figure 2d) can be easily conducted. This cell is thus suited for electrochemical experiments and simulates the operation of PEMFC.

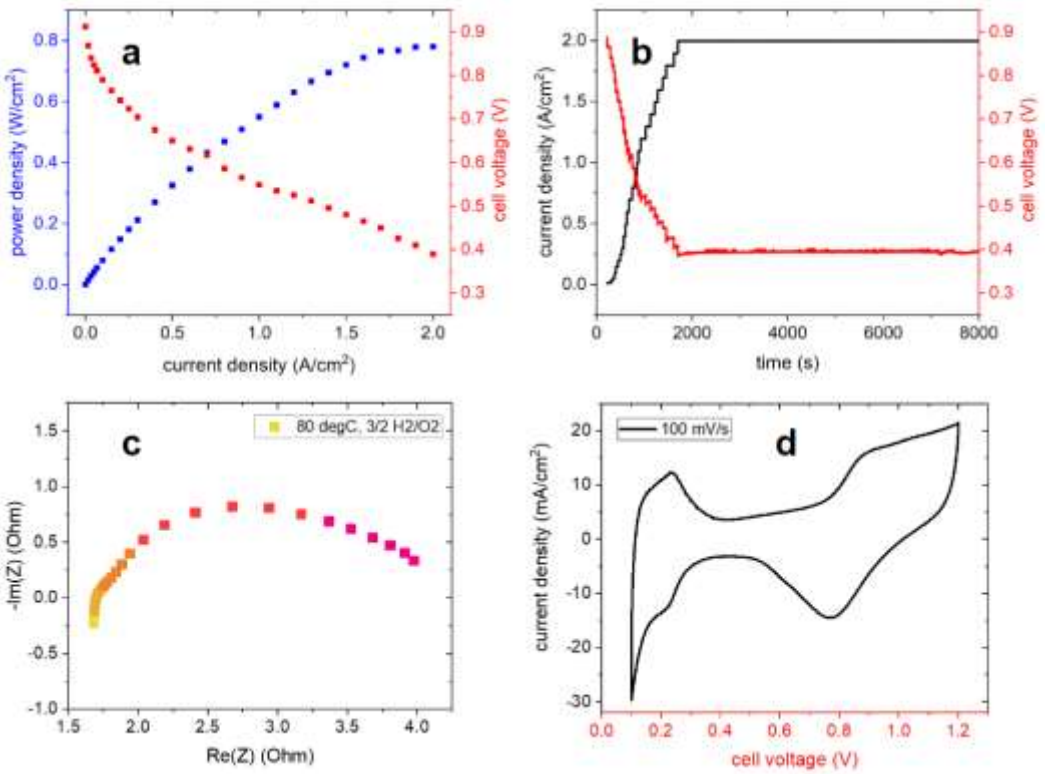

Figure 2: a) polarization curve [cell voltage (red) vs. current density (black)], and power density (blue) at 80°C under normal stoichiometry 3/2 sccm of H_2/O_2 on anode/cathode with 50% relative humidity, respectively; b) stability over 9h under high current density (black), cell voltage (red); c) PEIS before polarization curve under the same conditions, frequencies in range 100 kHz (yellow) to 10 Hz (pink) shown; d) ohmic-drop and hydrogen crossover compensated cyclic voltammetry with 100 mV/s scanrate at 50°C flowing 50/50 sccm of H_2/N_2 on anode/cathode with 70% relative humidity, respectively and hydrogen crossover 4 mA/cm^2. Cell voltages shown are IR corrected.

Angle-resolved X-ray emission spectroscopy

Setup and depth sensitivity

This cell aims to enable XAS in-situ/operando experiments of low-loading catalyst layers with an improved signal-to-noise ratio and depth sensitivity. It is accomplished using a 5-crystal analyzer placed on a Rowland circle roughly one meter in diameter. Although this setup significantly improves the spectral resolution, it reduces the overall flux to each crystal and makes it unsuitable for operando extended X-ray absorption fine structure (EXAFS) measurements. Nevertheless, the relatively wide groove opening of the cell allows placing a simple photodiode 2 cm from the sample, making the acquisition of lower-resolution EXAFS possible, however, at the expense of the depth resolution.

Our cell is primarily focused (but not limited) on PEMFC systems. In this contribution, we demonstrate its capabilities on a CCM with a PtNi catalyst containing only 0.017 mg_{Ni}/cm^2.

The diagram of the experimental setup is depicted in Figure 3a and Figure 3b shows the assembled version at the ID26 beamline. The incidence angle was fixed at -59° with respect

to the sample normal. We collect XAS spectra by selecting the Ni K-alpha fluorescence line with an emission spectrometer in Rowland geometry with five analyzer crystals [19]. The five-crystal analyzer covers an emission angle range from 49° to 77°, with crystal 5 (C5) being the most grazing.

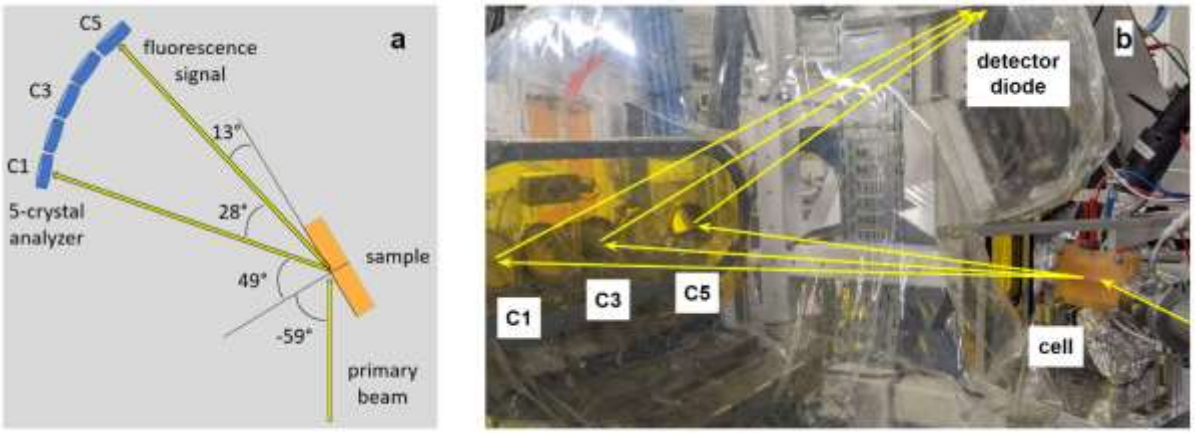

Figure 3: a) a sketch of the experimental setup with the hard X-ray emission spectrometer using five analyzer crystals (highlighted C1, C3, and C5), with the respective geometry; b) an actual setup at ID26 beamline ESRF

The standard high-resolution XAS (Figure 4) is obtained as the sum of the signal from all five crystals. Two contributions explain our system: metallic nickel Ni^0 (Ni foil) and ionic Ni^{2+} in Nafion (0.1 M $NiSO_4$ solution pipetted on the Nafion membrane). In our system, metallic nickel is present in the PtNi nanoparticles in the cathodic catalyst layer at the surface of the CCM. We have tried other references containing $Ni^{2+,}$ but only the $NiSO_4$ in Nafion showed the same fingerprint as this CCM spectrum. Thus, Ni^{2+} clearly comes from the ions dissolved in the ionomer.

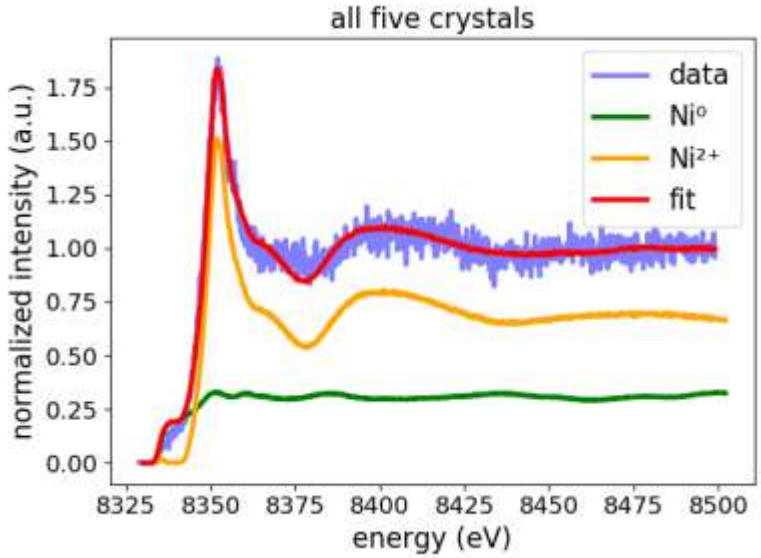

Figure 4: The XANES of Ni K-alpha edge spectrum (blue), fitted (red) as a linear combination of two reference data: metallic nickel Ni^0 (Ni foil) and ionic Ni^{2+} in Nafion (0.1 M $NiSO_4$ solution pipetted on the Nafion membrane)

The combination of this specific cell design with the crystal analyzer at low angular outrange enables depth sensitivity measurements. Thanks to the Lambert-Beer law of attenuation,

each crystal sees different ratios of surface-to-bulk information. X-ray fluorescence from Ni species within the bulk is more attenuated at grazing angles. Thus, less signal will reach crystal C5 than C1 from a specific species at a certain depth. For example, suppose Ni^{2+} species is in the bulk phase underneath a layer of metallic Ni^0. Then the grazing-angle C5 will have a high contribution from Ni^0 and a meager contribution of Ni^{2+}, thus a lower Ni^{2+}/Ni^0 ratio. On the other hand, the C1 at a normal angle will have the same Ni^0 contribution but more Ni^{2+} signal. Thus, the Ni^{2+}/Ni^0 ratio will be higher for C1 than for C5.

In other words, the C5 signal has a higher surface-to-bulk ratio and is more surface-sensitive. Vice versa, C1 is more bulk-sensitive. This can be observed by following the pre-edge spectral change from crystal 1 to 5 (Figure 5). We see that C1 (Figure 5a) has the lowest contribution of metallic Ni^0 (green), while C5 (Figure 5c) has the highest. This means that most of the metallic nickel should be on the surface, which is indeed the case as metallic nickel is present in the PtNi nanoparticles in the cathodic catalyst layer at the surface of the CCM. This provides strong evidence that we extract depth information about the system using this technique.

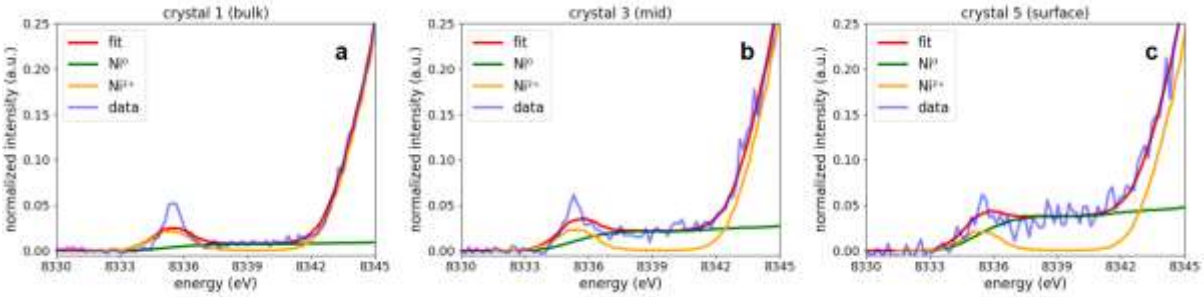

Figure 5: XES spectra of Ni K-alpha pre-edge fitted as a linear combination of metallic Ni^0 and ionic Ni^{2+} contributions for a) crystal 1, b) crystal 3, and c) crystal 5; The contribution of metallic Ni increases from C1 to C5 as Ni^0 is present in the cathode catalyst layer on the surface of the CCM.

Time-resolved in-situ experiment

Under an oxygen atmosphere, hard X-rays produce free radicals in the system, making the Nafion® ionomer in an operating PEMFC very sensitive to radiation damage. Thus, for in-situ measurements, we collected spectra only from C1, C3, and C5 to assess the evolution of each Ni species in time and depth by evaluating the Ni^{2+}/Ni^0 ratio (Figure 6). The first dataset at t = 0 h was acquired after an accelerated stress test (AST) (see supporting information for the exact protocol). After 2h at 0.5 V in H_2/O_2 we measured a second dataset and performed a CV (0.05 to 1.2) V to evaluate electrochemical performance. Consequently, we kept the cell at 0.5 V in H_2/O_2 for 2 more hours and acquired the third dataset. All the fitted spectra are in the supporting information.

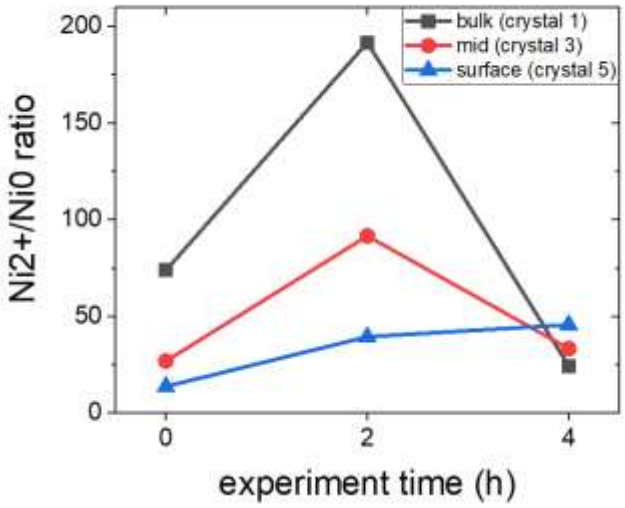

Figure 6: Time evolution of Ni^{2+}/Ni^{0} ratio. Coefficients were found using linear combination fitting. Time 0 h corresponds to the system after conditioning and AST. Then, the sample was held at 0.5 V in H_2/O_2 for 2h. Consequently, the same potential hold was repeated.

At t = 0 h, the highest Ni^{2+}/Ni^{0} ratio is for C1 (black), which means that most of the Ni^{2+} is in the bulk. Vice versa, the lowest Ni^{2+}/Ni^{0} ratio for C5 (blue) means that most of the Ni^{0} is at the surface. This is natural because the catalyst layer containing the most metallic Ni^{0} is above the Nafion membrane, where a significant fraction of Ni^{2+} is dissolved. After 2h of constant potential, the trend remains the same, but the ratios monotonically increase as more metallic Ni is dissolved out of the catalyst into the ionomer. Another possible explanation for the monotonic increase could be the movement of Ni^{2+} ions toward the cathode as they are dragged with protons from the Nafion membrane. Although we are unable to distinguish between the two processes at this point, a thorough experiment is foreseen to elucidate the movement and dissolution of Ni species.
Finally, after a total of 4h of the constant potential hold, the trend flips, and the bulk-sensitive crystal 1 shows the lowest Ni^{2+}/Ni^{0} ratio. This means that most of the metallic Ni^{0} signal now comes from the bulk (i.e., Nafion membrane), suggesting a formation of a metallic Ni band. Such a phenomenon was previously reported and studied for Pt [20], [21], [22], [23]. However, Ni reduction potential in an acidic solution is below -0.2 V [24] and thus should not occur within the operational boundaries of a fuel cell. Additionally, cations in ionomer affect the local pH, potentially changing it to an alkaline regime. We speculate that direct reduction by the hydrogen crossover together with a change in local pH is responsible for a direct reduction of Ni^{2+} ions in Nafion, or the reduction is caused by the X-ray radiation dose. From the current data, it is not possible to deconvolute these factors. Nevertheless, it is known that ions dissolved from the catalyst layer might have detrimental consequences for the performance of a hydrogen fuel cell as they slow down the diffusion coefficient of protons [25], [2]. Within this work, we have demonstrated the feasibility of angle-resolved XAS to resolve depth information about metallic and ionic transition metal species and their movements in an operating fuel cell.

Conclusions and Outlook

We have presented the design of a PEMFC optimized for angle-resolved X-ray absorption spectroscopy. The cell was designed for low-loading CCMs with a small sample size and minimal trade-offs in performance. We demonstrated the feasibility of depth-sensitive XAS by conducting an in-situ experiment with 0.017 mg_{Ni}/cm^2 PtNi-based CCM with a crystal analyzer. The experiment confirmed that Ni^{2+} is dissolved in the bulk of the Nafion membrane and that Ni^0 is present in the catalyst layer at the surface of the CCM. To distinguish between certain phenomena, such as the dissolution of Ni^0 to Ni^{2+} and the movement of Ni^{2+} towards the cathode, we aim to improve the temporal and depth resolution by incorporating a 2D detector. This will allow us to acquire XAS spectra from all five analyzer crystals simultaneously, and, together with advanced data analysis, will enable tracking the dynamic movement of the metallic species within the CCM in fuel cell operating conditions.

Acknowledgment

This project has received funding from the European Union's Horizon 2020 research and innovation program under the Marie Skłodowska-Curie grant agreement No 847439.
We acknowledge ESRF for enabling and supporting this research. Stored data [26] can be obtained upon request.

Bibliography

[1] L. Pan, S. Ott, F. Dionigi, P. Strasser, Current challenges related to the deployment of shape-controlled Pt alloy oxygen reduction reaction nanocatalysts into low Pt-loaded cathode layers of proton exchange membrane fuel cells, Current Opinion in Electrochemistry. 18 (2019) 61–71. https://doi.org/10.1016/j.coelec.2019.10.011.

[2] C. Lee, X. Wang, J.-K. Peng, A. Katzenberg, R.K. Ahluwalia, A. Kusoglu, S. Komini Babu, J.S. Spendelow, R. Mukundan, R.L. Borup, Toward a Comprehensive Understanding of Cation Effects in Proton Exchange Membrane Fuel Cells, ACS Appl. Mater. Interfaces. 14 (2022) 35555–35568. https://doi.org/10.1021/acsami.2c07085.

[3] P. Zimmermann, S. Peredkov, P.M. Abdala, S. DeBeer, M. Tromp, C. Müller, J.A. van Bokhoven, Modern X-ray spectroscopy: XAS and XES in the laboratory, Coord. Chem. Rev. 423 (2020) 213466. https://doi.org/10.1016/j.ccr.2020.213466.

[4] T.M. Arruda, B. Shyam, J.S. Lawton, N. Ramaswamy, D.E. Budil, D.E. Ramaker, S. Mukerjee, Fundamental Aspects of Spontaneous Cathodic Deposition of Ru onto Pt/C Electrocatalysts and Membranes under Direct Methanol Fuel Cell Operating Conditions: An in Situ X-ray Absorption Spectroscopy and Electron Spin Resonance Study, J. Phys. Chem. C. 114 (2010) 1028–1040. https://doi.org/10.1021/jp908082j.

[5] R. Viswanathan, G. Hou, R. Liu, S.R. Bare, F. Modica, G. Mickelson, C.U. Segre, N. Leyarovska, E.S. Smotkin, In-Situ XANES of Carbon-Supported Pt−Ru Anode Electrocatalyst for Reformate-Air Polymer Electrolyte Fuel Cells,

J. Phys. Chem. B. 106 (2002) 3458–3465. https://doi.org/10.1021/jp0139787.
[6] C. Roth, N. Martz, T. Buhrmester, J. Scherer, H. Fuess, In-situ XAFS fuel cell measurements of a carbon-supported Pt–Ru anode electrocatalyst in hydrogen and direct methanol operation, Phys. Chem. Chem. Phys. 4 (2002) 3555–3557. https://doi.org/10.1039/B204293B.
[7] R.J.K. Wiltshire, C.R. King, A. Rose, P.P. Wells, M.P. Hogarth, D. Thompsett, A.E. Russell, A PEM fuel cell for in situ XAS studies, Electrochim. Acta. 50 (2005) 5208–5217. https://doi.org/10.1016/j.electacta.2005.05.038.
[8] E. Principi, A. Di Cicco, A. Witkowska, R. Marassi, Performance of a fuel cell optimized for in situX-ray absorption experiments, J. Synchrotron Radiat. 14 (2007) 276–281. https://doi.org/10.1107/S0909049507013593.
[9] J. Li, M.T. Sougrati, A. Zitolo, J.M. Ablett, I.C. Oğuz, T. Mineva, I. Matanovic, P. Atanassov, Y. Huang, I. Zenyuk, A. Di Cicco, K. Kumar, L. Dubau, F. Maillard, G. Dražić, F. Jaouen, Identification of durable and non-durable FeNx sites in Fe–N–C materials for proton exchange membrane fuel cells, Nature Catalysis. 4 (2020) 10–19. https://doi.org/10.1038/s41929-020-00545-2.
[10] N. Ishiguro, S. Kityakarn, O. Sekizawa, T. Uruga, T. Sasabe, K. Nagasawa, T. Yokoyama, M. Tada, Rate Enhancements in Structural Transformations of Pt–Co and Pt–Ni Bimetallic Cathode Catalysts in Polymer Electrolyte Fuel Cells Studied by in Situ Time-Resolved X-ray Absorption Fine Structure, J. Phys. Chem. C. 118 (2014) 15874–15883. https://doi.org/10.1021/jp504738p.
[11] U.S. Drive, Fuel Cell Technical Team Roadmap, (2017). https://www.energy.gov/sites/default/files/2017/11/f46/FCTT_Roadmap_Nov_2017_FINAL.pdf.
[12] K. Isegawa, D. Kim, H. Kondoh, Chemical state changes of Nafion in model polymer electrolyte fuel cell under oxygen/hydrogen gas atmosphere observed by S-K XANES spectroscopy, RSC Adv. 8 (2018) 38204–38209. https://doi.org/10.1039/c8ra06426a.
[13] A.M. Baker, Y. Cai, J.M. Ziegelbauer, D. Agyeman-Budu, A. Woll, A. Kongkanand, R. Mukundan, R.L. Borup, Development of Operando Confocal Microprobe X-ray Fluorescence Techniques to Measure Cation Transport in PEM Fuel Cells, ECS Trans. 92 (2019) 107. https://doi.org/10.1149/09208.0107ecst.
[14] H. Matsui, N. Ishiguro, T. Uruga, O. Sekizawa, K. Higashi, N. Maejima, M. Tada, Operando 3D Visualization of Migration and Degradation of a Platinum Cathode Catalyst in a Polymer Electrolyte Fuel Cell, Angew. Chem. Int. Ed Engl. 56 (2017) 9371–9375. https://doi.org/10.1002/anie.201703940.
[15] C. Maurizio, M. Rovezzi, F. Bardelli, H.G. Pais, F. D'Acapito, Setup for optimized grazing incidence x-ray absorption experiments on thin films on substrates, Rev. Sci. Instrum. 80 (2009) 063904. https://doi.org/10.1063/1.3155791.
[16] Y. Wakisaka, H. Uehara, Q. Yuan, D. Kido, T. Wada, M. Uo, Y. Uemura, T. Yokoyama, Y. Kamei, S. Kuroda, A. Ohira, S. Takakusagi, K. Asakura, Extracting the local electronic states of Pt polycrystalline films surface under electrochemical conditions using polarization-dependent total reflection fluorescence x-ray absorption near edge structure spectroscopy, Electron. Struct. 2 (2020) 044003. https://doi.org/10.1088/2516-1075/abd1ca.
[17] Y. Kayser, J. Sá, J. Szlachetko, Depth-Resolved X-ray Absorption Spectroscopy by Means of Grazing Emission X-ray Fluorescence, Anal. Chem. 87 (2015) 10815–10821. https://doi.org/10.1021/acs.analchem.5b03346.

[18] S. Gunduz, D.J. Deka, J. Kim, M. Wilson, M. Warren, U.S. Ozkan, Incident-angle dependent operando XAS cell design: investigation of the electrochemical cells under operating conditions at various incidence angles, RSC Adv. 11 (2021) 6456–6463. https://doi.org/10.1039/d0ra09579f.
[19] P. Glatzel, A. Harris, P. Marion, M. Sikora, T.C. Weng, C. Guilloud, S. Lafuerza, M. Rovezzi, B. Detlefs, L. Ducotté, The five-analyzer point-to-point scanning crystal spectrometer at ESRF ID26, J. Synchrotron Radiat. 28 (2021) 362–371. https://doi.org/10.1107/S1600577520015416.
[20] W. Bi, G.E. Gray, T.F. Fuller, PEM Fuel Cell Pt／C Dissolution and Deposition in Nafion Electrolyte, Electrochem. Solid-State Lett. 10 (2007) B101. https://doi.org/10.1149/1.2712796.
[21] J. Péron, Y. Nedellec, D.J. Jones, J. Rozière, The effect of dissolution, migration and precipitation of platinum in Nafion®-based membrane electrode assemblies during fuel cell operation at high potential, J. Power Sources. 185 (2008) 1209–1217. https://doi.org/10.1016/j.jpowsour.2008.06.098.
[22] D. Zhao, B.L. Yi, H.M. Zhang, M. Liu, The effect of platinum in a Nafion membrane on the durability of the membrane under fuel cell conditions, J. Power Sources. 195 (2010) 4606–4612. https://doi.org/10.1016/j.jpowsour.2010.02.043.
[23] S. Helmly, B. Ohnmacht, P. Gazdzicki, R. Hiesgen, E. Gülzow, K.A. Friedrich, Influence of the distribution of platinum deposits on the properties and degradation of platinum-impregnated nafion membranes, J. Electrochem. Soc. 161 (2014) F1416–F1426. https://doi.org/10.1149/2.0531414jes.
[24] L.-F. Huang, M.J. Hutchison, R.J. Santucci Jr, J.R. Scully, J.M. Rondinelli, Improved Electrochemical Phase Diagrams from Theory and Experiment: The Ni–Water System and Its Complex Compounds, J. Phys. Chem. C. 121 (2017) 9782–9789. https://doi.org/10.1021/acs.jpcc.7b02771.
[25] A. Han, C. Fu, X. Yan, J. Chen, X. Cheng, C. Ke, J. Hou, S. Shen, J. Zhang, Effect of cobalt ion contamination on proton conduction of ultrathin Nafion film, Int. J. Hydrogen Energy. 45 (2020) 25276–25285. https://doi.org/10.1016/j.ijhydene.2020.06.205.
[26] J. Drnec, M. Ronovsky, M. Myllymäki, Following dissolved nickel from advanced Pt-alloyed ORR catalysts in a real fuel cell, (2025). https://doi.org/10.15151/ESRF-ES-764146616.